

# Experimental realization of a high-contrast grating based broadband quarter-wave plate

Mehmet Mutlu,<sup>1,2,\*</sup> Ahmet E. Akosman,<sup>1,2</sup> Gokhan Kurt,<sup>2</sup> Mutlu Gokkavas,<sup>2</sup> and Ekmel Ozbay<sup>1,2</sup>

<sup>1</sup>Department of Electrical and Electronics Engineering, Bilkent University, 06800 Ankara, Turkey

<sup>2</sup>Nanotechnology Research Center, Bilkent University, 06800 Ankara, Turkey

\*mutlu@ee.bilkent.edu.tr

**Abstract:** Fabrication and experimental characterization of a broadband quarter-wave plate, which is based on two-dimensional and binary silicon high-contrast gratings, are reported. The quarter-wave plate feature is achieved by the utilization of a regime, in which the proposed grating structure exhibits nearly total and approximately equal transmission of transverse electric and transverse magnetic waves with a phase difference of approximately  $\pi/2$ . The numerical and experimental results suggest a percent bandwidth of 42% and 33%, respectively, if the operation regime is defined as the range for which the conversion efficiency is higher than 0.9. A compact circular polarizer can be implemented by combining the grating with a linear polarizer.

© 2012 Optical Society of America

**OCIS codes:** (070.7345) Wave propagation; (050.2770) Gratings; (230.5440) Polarization-selective devices.

---

## References and links

1. V. Karagodsky and C. J. Chang-Hasnain, "Physics of near-wavelength high contrast gratings," *Opt. Express* **20**, 10888–10895 (2012).
2. C. Mateus, M. Huang, Y. Deng, A. Neureuther, and C. Chang-Hasnain, "Ultrabroadband mirror using low-index cladded subwavelength grating," *IEEE Photon. Technol. Lett.* **16**, 518–520 (2004).
3. C. Mateus, M. Huang, L. Chen, C. Chang-Hasnain, and Y. Suzuki, "Broad-band mirror (1.12–1.62  $\mu\text{m}$ ) using a subwavelength grating," *IEEE Photon. Technol. Lett.* **16**, 1676–1678 (2004).
4. V. Karagodsky, C. Chase, and C. J. Chang-Hasnain, "Matrix Fabry–Perot resonance mechanism in high-contrast gratings," *Opt. Lett.* **36**, 1704–1706 (2011).
5. M. C. Y. Huang, Y. Zhou, and C. J. Chang-Hasnain, "A surface-emitting laser incorporating a high-index-contrast subwavelength grating," *Nat. Photon.* **1**, 119–122 (2007).
6. M. C. Y. Huang, Y. Zhou, and C. J. Chang-Hasnain, "A nanoelectromechanical tunable laser," *Nat. Photon.* **2**, 180–184 (2008).
7. Y. Zhou, V. Karagodsky, B. Pesala, F. G. Sedgwick, and C. J. Chang-Hasnain, "A novel ultra-low loss hollow-core waveguide using subwavelength high-contrast gratings," *Opt. Express* **17**, 1508–1517 (2009).
8. V. Karagodsky, B. Pesala, F. G. Sedgwick, and C. J. Chang-Hasnain, "Dispersion properties of high-contrast grating hollow-core waveguides," *Opt. Lett.* **35**, 4099–4101 (2010).
9. F. Lu, F. G. Sedgwick, V. Karagodsky, C. Chase, and C. J. Chang-Hasnain, "Planar high-numerical-aperture low-loss focusing reflectors and lenses using subwavelength high contrast gratings," *Opt. Express* **18**, 12606–12614 (2010).
10. D. Fattal, J. Li, Z. Peng, M. Fiorentino, and R. G. Beausoleil, "Flat dielectric grating reflectors with focusing abilities," *Nat. Photon.* **4**, 466–470 (2010).

11. F. Brückner, D. Friedrich, T. Clausnitzer, M. Britzger, O. Burmeister, K. Danzmann, E.-B. Kley, A. Tünnermann, and R. Schnabel, "Realization of a monolithic high-reflectivity cavity mirror from a single silicon crystal," *Phys. Rev. Lett.* **104**, 163903 (2010).
12. W. Yang, F. Sedgwick, Z. Zhang, and C. J. Chang-Hasnain, "High contrast grating based saturable absorber for mode-locked lasers," in "Conference on Lasers and Electro-Optics," (Optical Society of America, 2010), p. CThI5.
13. M. Zohar, M. Auslender, L. Faraone, and S. Hava, "Novel resonant cavity-enhanced absorber structures for high-efficiency midinfrared photodetector application," *J. Nanophoton.* **5**, 051824 (2011).
14. H. Wu, W. Mo, J. Hou, D. Gao, R. Hao, R. Guo, W. Wu, and Z. Zhou, "Polarizing beam splitter based on a subwavelength asymmetric profile grating," *J. Opt.* **12**, 015703 (2010).
15. H. Wu, W. Mo, J. Hou, D. Gao, R. Hao, H. Jiang, R. Guo, W. Wu, and Z. Zhou, "A high performance polarization independent reflector based on a multilayered configuration grating structure," *J. Opt.* **12**, 045703 (2010).
16. W.-M. Ye, X.-D. Yuan, C.-C. Guo, and C. Zen, "Unidirectional transmission in non-symmetric gratings made of isotropic material," *Opt. Express* **18**, 7590–7595 (2010).
17. Y. Zhou, M. Huang, and C. Chang-Hasnain, "Large fabrication tolerance for VCSELs using high-contrast grating," *IEEE Photon. Technol. Lett.* **20**, 434–436 (2008).
18. M. Mutlu, A. E. Akosman, and E. Ozbay, "Broadband circular polarizer based on high-contrast gratings," *Opt. Lett.* **37**, 2094–2096 (2012).
19. V. Karagodsky, F. G. Sedgwick, and C. J. Chang-Hasnain, "Theoretical analysis of subwavelength high contrast grating reflectors," *Opt. Express* **18**, 16973–16988 (2010).
20. M. G. Moharam, E. B. Grann, D. A. Pommert, and T. K. Gaylord, "Formulation for stable and efficient implementation of the rigorous coupled-wave analysis of binary gratings," *J. Opt. Soc. Am. A* **12**, 1068–1076 (1995).
21. E. D. Palik, *Handbook of Optical Constants of Solids* (Academic, 1998).
22. M. Mutlu, A. E. Akosman, A. E. Serebryannikov, and E. Ozbay, "Asymmetric chiral metamaterial circular polarizer based on four U-shaped split ring resonators," *Opt. Lett.* **36**, 1653–1655 (2011).
23. C. A. Balanis, *Antenna Theory: Analysis and Design* (Wiley, 2005).
24. Z. Li, R. Zhao, T. Koschny, M. Kafesaki, K. B. Alici, E. Colak, H. Caglayan, and E. Ozbay, "Chiral metamaterials with negative refractive index based on four "U" split ring resonators," *Appl. Phys. Lett.* **97**, 081901 (2010).
25. S.-W. Ahn, K.-D. Lee, J.-S. Kim, S. H. Kim, J.-D. Park, S.-H. Lee, and P.-W. Yoon, "Fabrication of a 50 nm half-pitch wire grid polarizer using nanoimprint lithography," *Nanotechnology* **16**, 1874–1877 (2005).
26. D. W. C. So and S. R. Seshadri, "Thin-film grating polarizer," *Opt. Lett.* **19**, 469–471 (1994).
27. G. Schider, J. R. Krenn, W. Gotschy, B. Lamprecht, H. Ditlbacher, A. Leitner, and F. R. Aussenegg, "Optical properties of Ag and Au nanowire gratings," *J. Appl. Phys.* **90**, 3825–3830 (2001).

## 1. Introduction

High-contrast gratings (HCGs), which are near-wavelength binary grating structures consisting of a high-index grating material surrounded by low-index materials [1], have attracted significant interest since the numerical [2] and experimental [3] demonstration of their diffraction-free, broadband, and high-reflectivity regimes. Thereafter, the extraordinary and intriguing properties of HCGs have been exploited to design and build various optical elements such as high-Q Fabry-Perot resonators [4], top mirrors in vertical-cavity surface-emitting lasers [5, 6], one- and two-dimensional hollow-core low-loss optical waveguides [7], slow-light waveguides [8], planar focusing reflectors and lenses [9, 10], monolithic cavity mirrors [11], saturable absorbers [12], resonant cavity-enhanced absorbers [13], polarizing beam-splitters [14], polarization-independent reflectors [15], and unidirectional transmission devices [16]. Properties such as geometrical simpleness and flexibility, large fabrication tolerance [17], small footprint, and well-known theoretical description makes HCGs promising candidates for various practical applications.

In a recent study, we have shown that a two-dimensional HCG structure with optimized geometrical parameters can be utilized for implementing a broadband circular polarizer [18]. The optimized geometrical parameters have been suggested by benefiting from the periodic dielectric slab waveguide interpretation, which is studied rigorously in [19]. The spectral transmission results obtained from the rigorous coupled-wave analysis [20] and finite-difference time-domain (FDTD) simulations (FDTD Solutions, Lumerical Inc.) have suggested that an operation percent bandwidth of 54% and 51% can be achieved, respectively, under the assump-

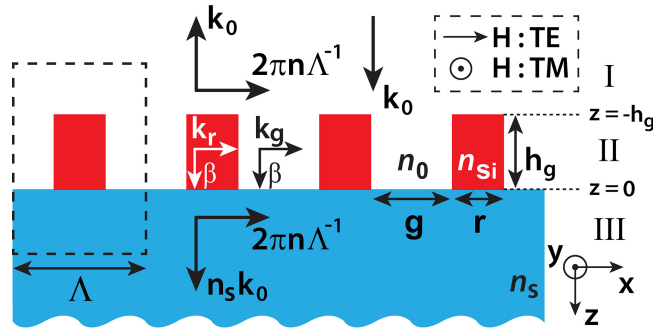


Fig. 1. Illustration of the proposed quarter-wave plate geometry. The dashed square box on the left denotes one period. The geometrical parameters are given by  $r = 220$  nm,  $g = 350$  nm,  $h_g = 320$  nm, and  $\Lambda = 570$  nm. In the theoretical and numerical consideration, for the sake of simplicity, regions I and III are assumed to be infinite in the  $-z$  and  $+z$  directions, respectively. The materials constituting region III and the ridges in region II are sapphire and silicon, respectively, whereas region I is free-space.  $n_0$ ,  $n_{si}$ , and  $n_s$  represent the refractive indices of free-space, silicon, and sapphire, respectively. *Grating direction* is defined such that it corresponds to the  $y$  direction.

tion that the proposed structure is said to be within the operation regime if the conversion efficiency exceeds 0.9. For the sake of maximizing the operation bandwidth in this theoretical study, the material that is employed outside the grating region as well as in the grooves between the silicon gratings has been assumed to be silicon dioxide.

## 2. Proposed Geometry

In this paper, we study the potential of the experimental realization and characterization of an HCG based broadband quarter-wave plate that can be designed by following the methodology given in [18]. By considering the potential challenges in the fabrication stage and evaluating the limitations of the devices used in the nanofabrication processes, without sacrificing significantly from the bandwidth, we decided to design an HCG structure with sapphire substrate and silicon gratings, where the grooves between the gratings are free-space as well as the region that the wave is incident onto the structure from. The proposed geometry is depicted in Fig. 1. The polarization states are defined such that a plane wave is transverse electric (TE) and transverse magnetic (TM) polarized if the magnetic field is in the  $x$  and  $y$  directions, respectively, where the incident wave propagates in the  $+z$  direction.

In the present study, a theoretical solution of the specific HCG design problem is not provided due to the fact that the solution is fundamentally the same as the ones given in [18, 19]. However, we make a remark on the difference of this problem compared to the previously mentioned studies. As a result of the selection of different materials for filling regions I and III, i.e., free-space and sapphire, respectively, the wavenumbers of the zeroth reflection and transmission orders are expected to be different. The wavenumber of the zeroth reflection order is equal to  $k_0$  and given by  $\gamma_{0,I} = 2\pi\lambda_0^{-1}$ , whereas the wavenumber of the zeroth transmission order is equal to  $n_s k_0$  and, therefore, given by  $\gamma_{0,III} = 2\pi n_s \lambda_0^{-1}$ . This discrepancy results in unequal lateral magnetic field distributions in regions I and III [denoted by  $H^I(x, z \leq -t_g)$  and  $H^{III}(x, z \geq 0)$  in [19], respectively]. Therefore, ensuring the utilization of the correct lateral distributions while matching the boundary conditions at  $z = -h_g$  and  $z = 0$  is of crucial importance and requires special attention.

The optimized HCG design is achieved with the aid of the theoretical calculations and the

rigorous coupled-wave analysis for vertical binary gratings [20]. The utilized geometrical parameters are provided in the caption of Fig. 1. Subsequently, FDTD simulations (FDTD Solutions, Lumerical Inc.) are run in order to numerically characterize the transmission of the proposed HCG structure for TM and TE waves, while taking the effects arising because of the material dispersion into account, i.e., dependence of  $n_{\text{si}}$  and  $n_{\text{s}}$  on the wavelength of the incident light. In the simulations, the refractive index data given in [21] is employed for  $n_{\text{si}}$  and  $n_{\text{s}}$ . The two-dimensional simulations are constructed such that the periodic boundary condition is employed along the  $x$  direction, whereas the perfectly matched layer (PML) boundary condition is adopted along the  $z$  direction. The sapphire substrate is assumed to be extending to infinity in the  $+z$  direction for the purpose of avoiding the oscillations in the transmission spectrum that originate because of the Fabry-Perot modes created within a substrate of a finite thickness. Moreover, as a result of the typical short coherence length of broadband light sources, such an effect is not expected to be visible in the experimental results, unless a substrate with a thickness that is comparable to the operation wavelength is employed.

### 3. Numerical Results

The numerically obtained normalized transmitted intensities for the HCG for normally incident TM and TE waves ( $|T_{\text{TM}}|^2$  and  $|T_{\text{TE}}|^2$ , respectively) are shown in Fig. 2(a). The proposed HCG geometry is optimized such that, in the close neighborhood of  $\lambda_0 = 1.55 \mu\text{m}$ , the conditions  $|T_{\text{TM}}| \simeq |T_{\text{TE}}|$  and  $\angle(T_{\text{TM}}) - \angle(T_{\text{TE}}) \simeq \pi/2$  are satisfied simultaneously, which result in the transmission of a right-hand circularly polarized (RCP, +) and left-hand circularly polarized (LCP, -) wave assuming that the structure is illuminated by a normally incident plane wave that is linearly polarized with a polarization plane angle of  $45^\circ$  and  $-45^\circ$  with respect to the  $x$ -axis on the  $xy$ -plane, respectively. The circular conversion coefficients for  $45^\circ$  polarization angle are subsequently calculated by  $C_{\pm} = 0.5(T_{\text{TM}} \mp iT_{\text{TE}})$  [22] and shown in Fig. 2(b). Obviously,  $T_{\text{TM}}$  and  $T_{\text{TE}}$  are complex numbers, which carry the phase information besides the magnitude. However, in the present experimental study, the phases of the numerical transmission coefficients

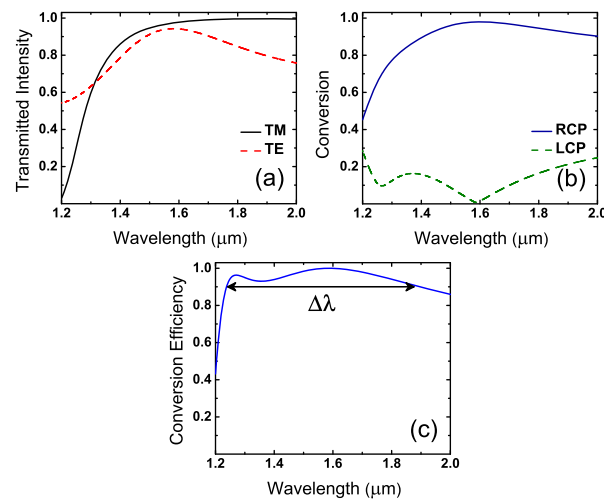


Fig. 2. Numerical (a) TM and TE transmitted intensities, (b) circular conversion coefficients, and (c) conversion efficiency spectrum obtained via FDTD simulations. The wavelength interval of operation is denoted by  $\Delta\lambda$ . The numerical conversion efficiency spectrum yields a percent bandwidth of 42%.

are not explicitly given, since the phase information is not required for the obtaining of the experimental conversion coefficients. Instead, as it will be evident subsequently, these coefficients can directly be measured by the utilization of a linear polarizer and a quarter-wave plate. Finally, the conversion efficiency, which is shown in Fig. 2(c), is calculated as follows [18]:

$$C_{\text{eff}} = \frac{|C_+|^2 - |C_-|^2}{|C_+|^2 + |C_-|^2}. \quad (1)$$

At this point, we impose a condition on  $C_{\text{eff}}$  such that the proposed structure is said to be in the operation regime if  $C_{\text{eff}} \geq 0.9$  is satisfied. This condition implies that, at the output interface, the intensity of the RCP wave should be, at least, 12.8 dB larger than that of the LCP wave. The numerical results suggest that the  $C_{\text{eff}}$  condition is satisfied between  $\lambda_0 = 1.24 \mu\text{m}$  and  $1.90 \mu\text{m}$ , which corresponds to a percent bandwidth of 42%, if the percent bandwidth is defined as follows [23]:

$$\text{BW}\% = 200\% \frac{\lambda_H/\lambda_L - 1}{\lambda_H/\lambda_L + 1}, \quad (2)$$

where  $\lambda_H$  and  $\lambda_L$  represent the higher and lower corners of the operation band, respectively. It is noteworthy that in the case of illumination by a plane wave with a polarization plane angle of  $-45^\circ$ ,  $C_+$  and  $C_-$  would simply be swapped.

In addition to the conversion efficiency interpretation, one can define the conversion characteristics of the proposed design by calculating the ellipticity spectrum for transmitted waves. Under the assumption that the HCG is illuminated by a normally incident plane wave with a polarization plane angle of  $\pm 45^\circ$ , the ellipticity,  $\eta$ , can be calculated as follows [24]:

$$\eta = \arctan \left( \frac{|C_+| - |C_-|}{|C_+| + |C_-|} \right). \quad (3)$$

By combining Eqs. (1) and (3),  $\eta$  can simply be calculated from the  $C_{\text{eff}}$  spectrum as follows:

$$\eta = \arctan \left( \frac{\sqrt{(1 + C_{\text{eff}})/(1 - C_{\text{eff}})} - 1}{\sqrt{(1 + C_{\text{eff}})/(1 - C_{\text{eff}})} + 1} \right). \quad (4)$$

Using Eq. (4), it can be shown that a conversion efficiency of 0.9 corresponds to  $\eta = 32^\circ$ . Finally, due to the one-to-one correspondence between  $\eta$  and  $C_{\text{eff}}$ , only the  $C_{\text{eff}}$  spectrum is provided in the present study.

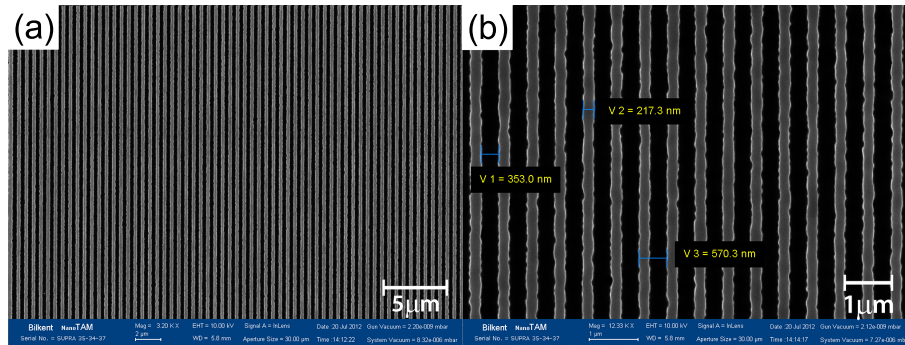


Fig. 3. (a) Zoomed out and (b) zoomed in top view SEM micrographs of the fabricated HCG structure. In (b), the legends V1, V2, and V3 denote the geometrical parameters  $g$ ,  $r$ , and  $\Lambda$ , respectively.

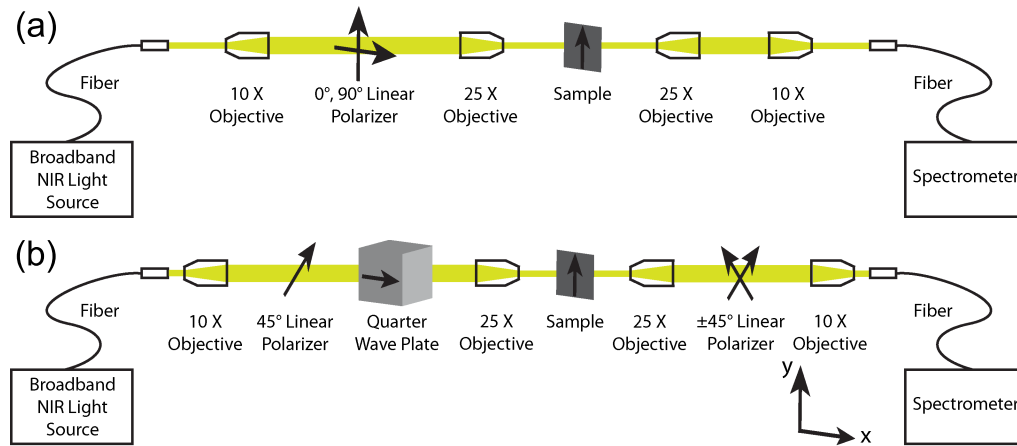


Fig. 4. Visual illustrations of the experimental setups that are utilized for the measurement of (a) linear transmission coefficients and (b) circular conversion coefficients. The arrows, which lie inside the HCG samples and point upwards, denote the grating direction that is defined in the caption of Fig. 1.

#### 4. Fabrication

The grating structure is fabricated onto a silicon-on-sapphire (SOS) wafer with a 100 mm diameter, which is purchased from Valley Design Corporation. The wafer consists of a  $600 \pm 60$  nm thick  $\langle 100 \rangle$  silicon layer that is grown epitaxially on a  $0.53 \pm 0.05$  mm thick R-plane sapphire. Firstly, the SOS wafer is diced into square shaped chips with the dimension of 6 mm by 6 mm. The fabrication process starts with the reduction of the thickness of the silicon layer to 320 nm by means of the reactive ion etching (RIE) technique, while using sulfur hexafluoride ( $\text{SF}_6$ ) as the etchant gas. Afterwards, polymethyl methacrylate (PMMA), which is an electron beam sensitive photoresist, is spun onto the sample. Subsequently, the desired grating structure is patterned onto the SOS sample using e-beam lithography. Following the development operation of the PMMA, the final step is accomplished by etching the unexposed silicon regions using the RIE system. The scanning electron microscope (SEM) micrographs of the fabricated HCG sample are shown in Fig. 3.

#### 5. Experimental Setup

The outlines of the two experimental setups, which are constructed for the measurement of the linear transmission coefficients and the circular conversion coefficients of the HCG sample, are illustrated in Fig. 4 in detail. In the experiments, the sample is illuminated by a broadband near-infrared (NIR) light source (Spectral Products, ASBN-W100-F-L) and, with the aid of standard commercial NIR objectives and an adjustable aperture (not shown in Fig. 4), the spot size of the incident light is adjusted to be  $50 \mu\text{m}$ . The normalization of the transmitted fields is performed with respect to a solely sapphire region that is obtained by etching the silicon layer on the SOS chip.

In the first measurement, which is illustrated in Fig. 4(a), the linear intensity transmission coefficients ( $|T_{\text{TM}}|^2$  and  $|T_{\text{TE}}|^2$ ) are obtained by the utilization of an adjustable linear polarizer (Thorlabs, DGL10) that is used for enabling the illumination of the grating region with TM and TE polarized light. In the second measurement, which is illustrated in Fig. 4(b) and conducted with the purpose of measuring the circular conversion coefficients, the grating region

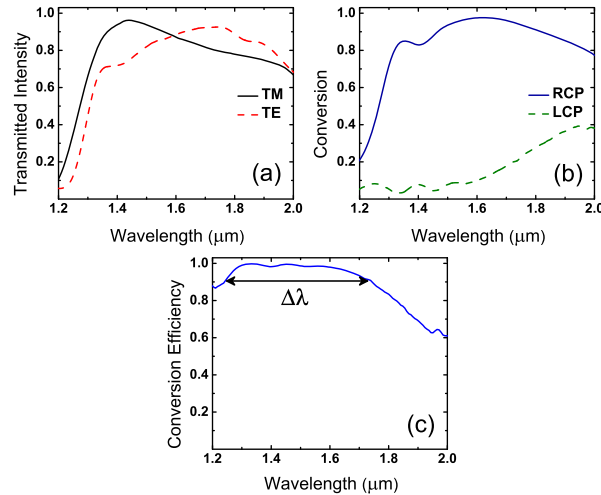


Fig. 5. Experimentally obtained (a) TM and TE transmitted intensities, (b) circular conversion coefficients, and (c) conversion efficiency spectrum. The wavelength interval of operation is denoted by  $\Delta\lambda$ . The experimental conversion efficiency spectrum yields a percent bandwidth of 33%.

is illuminated by an RCP wave as a result of the employment of an adjustable linear polarizer (with its transmission axis making a  $45^\circ$  angle with the  $x$  – axis) followed by a quarter-wave plate (Thorlabs, WPQ05M-1550) that is oriented such that its fast axis is along the  $x$  direction. At the farfield, the transmitted wave through the grating region is passed through an adjustable linear polarizer that is oriented such that its transmission axis makes angles of  $+45^\circ$  and  $-45^\circ$  with respect to the  $x$  – axis. Afterwards, the intensities of the waves that are transmitted through the linear polarizer are measured using the spectrometer (Ocean Optics, NIR256-2.5) in order to find the square of the magnitudes of the RCP and LCP conversion coefficients ( $|C_+|^2$  and  $|C_-|^2$ ), respectively. By the utilization of the Jones matrix formalism, it can easily be shown that by adjusting the linear polarizer to  $+45^\circ$  and  $-45^\circ$ ,  $|C_+|^2$  and  $|C_-|^2$  can be measured directly, respectively. As a result of the period of the proposed HCG structure being equal to  $570$  nm, FDTD simulations and experiments are conducted between the free-space wavelengths of  $1.2 \mu\text{m}$  and  $2 \mu\text{m}$  with the purpose of avoiding the wavelengths for which the HCG is diffractive, i.e.,  $\lambda_0 < n_s\Lambda$ .

The proposed HCG based quarter-wave plate can be combined with a HCG based [14], a wire grid [25], a thin-film grating [26], or a plasmonic [27] linear polarizer for the purpose of implementing a compact circular polarizer.

## 6. Experimental Results

The linear intensity transmission and circular conversion coefficients (for an incident wave with a polarization plane angle of  $45^\circ$ ), and the conversion efficiency spectrum obtained from the experiments are shown in Fig. 5. Conversion efficiency data given in Fig. 5(c) suggests that the experimental lower and higher corner wavelengths are obtained as  $\lambda_L = 1.25 \mu\text{m}$  and  $\lambda_H = 1.75 \mu\text{m}$ . The usage of Eq. (2) results in an experimental percent bandwidth of 33%. In spite of the achievement of a smaller percent bandwidth compared to the numerical predictions, the experimental results exhibit a good agreement with the numerical results shown in Fig. 2.

We conjecture that the most significant factors responsible from the discrepancies between the numerical and experimental results are finite-size effect and finite substrate thickness.

Finite-size effect originates from the usage of finite number of periods and finite grating length in the experiments (in contradiction with the two-dimensional periodic FDTD simulations, where the number of periods and the grating length are infinite) and possibly modifies the lateral and longitudinal wavenumbers of the excited modes inside region II and, additionally, this effect can result in diffraction from the edges of the sample. The utilization of a substrate with a finite thickness can result in multiple back-reflections inside the substrate, modifying the overall behavior of the corrugated surface and, in addition, Fresnel reflection from the back-side of the substrate can also modify the transmission characteristics of the sample.

In addition to the aforementioned effects, the trapezoidal grating profile achieved after the final etch step and possible deviations of the geometric parameters of the fabricated sample from the design parameters can conduce to the discrepancies between the numerical and experimental results. Furthermore, less significant effects such as the employment of non-ideal optical elements, i.e., linear polarizer and quarter-wave plate, probable small deviation of the actual refractive indices from the ones adopted in the simulations, and human related errors while setting the polarizer transmission axis angle and the angle of incidence might as well contribute to the deviations in the experimental results from the numerical ones.

## 7. Conclusions

In conclusion, we have shown the fabrication and the experimental characterization of a broadband quarter-wave plate that is based on two-dimensional silicon HCGs, where sapphire is employed as the substrate. It has been shown that a conversion efficiency that is higher than 0.9 can be achieved in a percent bandwidth of 42% and 33% numerically and experimentally, respectively. RCP and LCP waves can be obtained by adjusting the transmission axis of the linear polarizer to  $45^\circ$  and  $-45^\circ$  with respect to the  $x$ -axis, respectively. In terms of practical applicability, the proposed structure can be employed in laser and nanoantenna applications, liquid crystal displays, and remote sensors.

## Acknowledgments

The authors would like to thank Adil Burak Turhan for the e-beam lithography process and Yasemin Kanli for the initial FTIR measurements. This work is supported by the projects DPT-HAMIT, ESF-EPIGRAT and NATO-SET-181, and TUBITAK under the Project Nos. 107A004, 109A015, and 109E301. One of the authors (E. Ozbay) also acknowledges partial support from the Turkish Academy of Sciences.